RAA 2015 Vol. **15** No. **8**, 1264–1274 doi: 10.1088/1674–4527/15/8/011
http://www.raa-journal.org *http://www.iop.org/journals/raa*

Research in Astronomy and Astrophysics

Discovery of a strongly r-process enhanced extremely metal-poor star LAMOST J110901.22+075441.8

Hai-Ning Li[1], Wako Aoki[2,3], Satoshi Honda[4], Gang Zhao[1], Norbert Christlieb[5] and Takuma Suda[6]

[1] Key Laboratory of Optical Astronomy, National Astronomical Observatories, Chinese Academy of Sciences, Beijing 100012, China; *lhn@nao.cas.cn*
[2] National Astronomical Observatory of Japan, 2-21-1 Osawa, Mitaka, Tokyo, 181-8588, Japan
[3] Department of Astronomical Science, School of Physical Sciences, The Graduate University of Advanced Studies (SOKENDAI), 2-21-1 Osawa, Mitaka, Tokyo 181-8588, Japan
[4] University of Hyogo, Center for Astronomy, Nishigaichi, Sayo-cho, Sayo, Hyogo, 679-5313, Japan
[5] Zentrum für Astronomie der Universität Heidelberg, Landessternwarte, Königstuhl 12, D-69117 Heidelberg, Germany
[6] Research Center for the Early Universe, The University of Tokyo, Hongo 7-3-1, Bunkyo-ku, Tokyo 113-0033, Japan

Received 2015 April 1; accepted 2015 May 13

Abstract We report the discovery of an extremely metal-poor (EMP) giant, LAMOST J110901.22+075441.8, which exhibits a large excess of r-process elements with [Eu/Fe] $\sim +1.16$. The star is one of the newly discovered EMP stars identified from the LAMOST low-resolution spectroscopic survey and a high-resolution follow-up observation with the Subaru Telescope. Stellar parameters and elemental abundances have been determined from the Subaru spectrum. Accurate abundances for a total of 23 elements including 11 neutron-capture elements from Sr through Dy have been derived for LAMOST J110901.22+075441.8. The abundance pattern of LAMOST J110901.22+075441.8 in the range of C through Zn is in line with the "normal" population of EMP halo stars, except that it shows a notable underabundance in carbon. The heavy element abundance pattern of LAMOST J110901.22+075441.8 is in agreement with other well studied cool $r-$II metal-poor giants such as CS 22892−052 and CS 31082−001. The abundances of elements in the range from Ba through Dy match the scaled solar r-process pattern well. LAMOST J110901.22+075441.8 provides the first detailed measurements of neutron-capture elements among $r-$II stars at such low metallicity with [Fe/H] $\lesssim -3.4$, and exhibits similar behavior as other $r-$II stars in the abundance ratio of Zr/Eu as well as Sr/Eu and Ba/Eu.

Key words: star: abundances — stars: Population II — nucleosynthesis

1 INTRODUCTION

Detailed elemental abundances of metal-poor stars in the Galactic halo provide fundamental knowledge about the history and nature of nucleosynthesis in the Galaxy. Particularly, abundances of slow (s) and rapid (r) neutron-capture elements are of great importance to constrain early Galactic nucleosynthesis and chemical evolution models. In the past decades, great efforts have been devoted to studies in relevant fields based on high-resolution spectroscopic measurements of the elemental abundances of metal-poor stars in the Galaxy. These observations together with theoretical studies have revealed that the r-process was primarily responsible for the production of heavy elements beyond the iron group (Spite & Spite 1978; Sneden et al. 1996) in the early Galaxy. Only at later times (with higher metallicities) does the onset of the s-process occur, injecting nucleosynthesis material into the interstellar medium from long-lived low- and intermediate mass stars (Burris et al. 2000). Detections of radioactive elements including thorium and uranium in a few r-process enhanced metal-poor stars have provided an independent measurement on the age of these oldest stars, and hence set lower limits to the age of the Galaxy (Hill et al. 2002; Frebel et al. 2007).

Sneden et al. (1994) found the first r-process enhanced extremely metal-poor (EMP) giant CS 22892$-$052, with a [Eu/Fe] $\sim +1.6$ [1] and an abundance pattern from Ba through Dy which is similar to a scaled Solar System r-process (SSr) distribution. A few rare stars have subsequently been found to exhibit extreme enhancements in r-process elements, suggesting that the observed abundances are dominated by the effect from a single or very few nucleosynthesis events. Based on the definition by Beers & Christlieb (2005), such stars with [Eu/Fe] $> +1$ and [Ba/Eu] < 0 are referred to as $r-$II stars. Although the astrophysical site of the r-process is not yet clear, the r-process is believed to be connected to explosive conditions of massive-star core-collapse supernovae (Woosley et al. 1994), or neutron star mergers (Goriely et al. 2013). Therefore, $r-$II stars are the best candidates to explore the details of the r-process and the site where it occurs.

There are 12 $r-$II stars known to date (e.g., Hill et al. 2002; Sneden et al. 2003; Honda et al. 2004; Sneden et al. 2008; Hayek et al. 2009; Mashonkina et al. 2010; Aoki et al. 2010). Detailed abundance analysis of these $r-$II stars has found an ***excellent match between the stellar and solar r-process pattern in the Ba-Hf range***, which indicates a universal r-process, i.e. elements were produced with the same proportions during the evolution of the Galaxy. Such a conclusion is of fundamental importance for a better understanding of the nature of the r-process. To establish the origin of heavy elements beyond the iron group among the oldest stars in the Galaxy, larger samples with accurate measurements of additional elements are required.

LAMOST J110901.22+075441.8 was identified as a candidate of an EMP star from the first data release (Luo et al. 2015) of the low-resolution ($R \sim 1800$) spectroscopic survey of LAMOST [2] (the Large sky Area Multi-Object fiber Spectroscopic Telescope, also known as a Wang-Su Reflecting Schmidt Telescope or the Guo Shou Jing Telescope; Zhao et al. 2006; Cui et al. 2012; Zhao et al. 2012; Luo et al. 2012; Liu et al. 2015). The follow-up high-resolution spectroscopic observation was carried out with the Subaru Telescope (Li et al. 2015b), which has confirmed it is an $r-$II EMP giant.

In this paper, we introduce the observation and measurements of parameters and abundances of LAMOST J110901.22+075441.8 in Section 2; results and interpretations on the elemental abundance are presented in Section 3; patterns of heavy elements and conclusions are described in Sections 4 and 5 respectively.

[1] $[A/B] = \log(N_A/N_B)_\star - \log(N_A/N_B)_\odot$, where N_A and N_B are the number densities of elements A and B respectively, and $\star$ and $\odot$ refer to the star and the Sun respectively.

[2] See *http://www.lamost.org* for more detailed information, and a description of progress related to the LAMOST surveys.

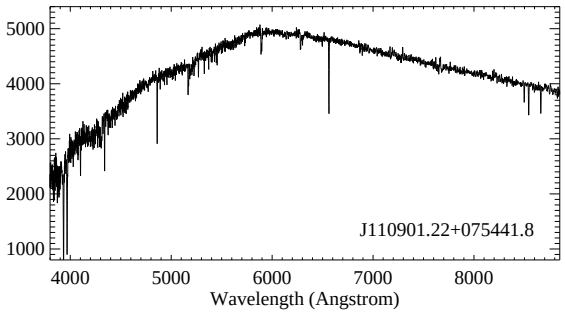

Fig. 1 The low-resolution spectrum of the r-II star obtained by LAMOST.

2 OBSERVATIONS AND MEASUREMENTS

2.1 Target Selection and Follow-up Observations

The wavelength coverage (3700–9100 Å) and resolving power ($R = 1800$) of LAMOST spectra (Fig. 1) allow a robust estimation of stellar parameters including metallicities. Methods to determine the metallicity of an object and the selection of EMP candidates were similar to those made by Li et al. (2015).

For 54 candidates of EMP stars selected from the LAMOST sample, "snapshot" high-resolution spectra were acquired with a resolving power $R = 36\,000$ and exposure times of 10−20 minutes during a two-night run in May 2014 with the Subaru/High Dispersion Spectrograph (HDS), which adopted the same method of observation as made by Aoki et al. (2013). LAMOST J110901.22+075441.8 was observed on May 9. Since this object is relatively bright (r = 12.08), quite a high signal-to-noise ratio (S/N) was achieved covering 4000−6800 Å, e.g., with an S/N of about 70 at 4500 Å and 110 at 5200 Å from an exposure of 10 minutes. Data reduction was carried out with standard procedures using the IRAF echelle package including bias-level correction, scattered light subtraction, flat-fielding, extraction of spectra and wavelength calibration using Th−Ar arc lines. Cosmic-ray hits were removed by the method described in Aoki et al. (2005).

Radial velocities of the sample were obtained using the `IRAF` procedure `fxcor`, and a synthetic spectrum with low-metallicity was employed as a template for cross-correlation. The above method derived a radial velocity of $-72.3 \pm 0.4\,\mathrm{km\,s^{-1}}$.

2.2 Stellar Parameters

Equivalent widths were measured by fitting Gaussian profiles to isolated atomic absorption lines based on the line list of Aoki et al. (2013) for elements lighter than Zn, and that from Mashonkina et al. (2010) for heavy elements beyond Sr.

Since there is not yet a uniform photometric system for all of the LAMOST input catalog, we have adopted a spectroscopic method to derive stellar parameters for the whole sample, including LAMOST J110901.22+075441.8. By minimizing the trend in the relationship between derived abundances and excitation potentials of Fe I lines, the effective temperature $T_{\rm eff}$ of LAMOST J110901.22+075441.8 was determined. The empirical formula derived by Frebel et al. (2013) has been adopted to correct the usually expected systematic offsets between the spectroscopic and photometric effective temperatures, which resulted in a $T_{\rm eff}$ of 4441 K compared to the original value of 4190 K. The microturbulent velocity ξ was also determined based on an analysis of Fe I lines, i.e., by forcing the iron abundances of individual lines to exhibit no dependence on the reduced equivalent widths. The sufficiently high quality of the Subaru spectrum allows us to detect 11 Fe II

lines for LAMOST J110901.22+075441.8. Therefore, the surface gravity $\log g$ was determined by minimizing the difference between the average abundances derived from the Fe I and Fe II lines.

The derived parameters of LAMOST J110901.22+075441.8 are listed in Table 1. Since the $V - K$ color is available for LAMOST J110901.22+075441.8 ($(V - K)_0 = 2.54$), we have also checked the photometric temperature of this object. Adopting the calibration by Alonso et al. (1999, 2001), the derived temperature is 4560 K, which is consistent with the spectroscopic temperature within the level of the uncertainty in our measurement.

2.3 Abundance Determination

For the abundance analysis, the 1D plane-parallel, hydrostatic model atmospheres of the ATLAS NEWODF grid of Castelli & Kurucz (2003) were adopted, assuming a mixing-length parameter of $\alpha_{\rm MLT} = 1.25$, no convective overshooting, and local thermodynamic equilibrium (LTE). An updated version of the abundance analysis code MOOG (Sneden 1973) was used, which does not treat continuous scattering as true absorption, but as a source function which sums both absorption and scattering (Sobeck et al. 2011). When calculating [X/H] and [X/Fe] abundance ratios, the photospheric solar abundances of Asplund et al. (2009) were adopted.

Abundances of most elements were computed using the measured equivalent widths of isolated atomic lines with the derived stellar parameters. For heavy elements whose spectral lines show hyperfine splitting, such as Sr, Ba, La and Eu, the elemental abundances were determined using spectral synthesis taking into account the isotopic splitting and/or hyperfine structure (HFS). The derived abundances of LAMOST J110901.22+075441.8 are listed in Table 1, which also include N, the number of lines which have been used to determine the abundance, together with the abundance error as described in the following text.

The uncertainties in the derived abundances mainly come from two aspects, i.e. the uncertainties in the equivalent width measurements and the uncertainties in stellar parameters. In the case of equivalent width measurement, when $N > 2$ lines of individual species of an element were observed, the dispersion around the average abundance was used to represent random error; if the elemental abundance was determined from a single line, the statistical error of the equivalent widths was estimated based on the classical formula of Cayrel (1988, eq. 7). The uncertainties in abundance associated with uncertainties in stellar parameters were estimated by individually varying $T_{\rm eff}$ by $+150$ K, $\log g$ by $+0.1$ dex and ξ by $+0.1\,{\rm km\,s^{-1}}$ in the stellar atmospheric model. The total uncertainty in the errors was computed as the quadratic sum of the above aspects, and is shown in the column for σ in Table 1.

3 ELEMENTAL ABUNDANCES AND INTERPRETATIONS

In Figure 2, abundance ratios relative to iron for LAMOST J110901.22+075441.8 are shown and compared to other metal-poor $r-$II stars, as well as "normal" metal-poor giants from the "First Stars" project (Cayrel et al. 2004). Note that there is only one cool metal-poor, main-sequence $r-$II star discovered by Aoki et al. (2010) with [Fe/H] $= -3.36$, while the rest are all cool giants.

3.1 Lithium through Zinc

Lithium. The Li I 6708 Å line is covered in the observed spectrum, but we could not detect the lithium line in LAMOST J110901.22+075441.8. An upper limit of A(Li) < 0.35 [3] has been derived based on spectral synthesis. This is not unexpected for a red giant which usually shows a rather low abundance of Li, since such objects have already undergone the first dredge-up and the surface material is mixed with internal material which is depleted in lithium.

[3] A(Li) is defined as $A({\rm Li}) = \log(N({\rm Li})/N({\rm H})) + 12$.

Table 1 Stellar Parameters and Elemental Abundances of LAMOST J110901.22+075441.8

	LAMOST J110901.22+075441.8				Sun
$T_{\rm eff}$(K)	4440±150				
$\log g$	0.70±0.1				
[Fe/H]	−3.41±0.1				
ξ(km s^{-1})	1.98±0.1				
Ion	$\log\epsilon$(X)	[X/Fe]	N	σ	$\log\epsilon$(X)
C	4.45	−0.57	1	0.38	8.43
Na	3.41	0.58	2	0.23	6.24
Mg	4.60	0.41	4	0.15	7.60
Si	4.58	0.48	1	0.17	7.51
Ca	3.30	0.31	15	0.16	6.34
Sc	−0.33	−0.07	8	0.16	3.15
Ti I	1.71	0.17	10	0.23	4.95
Ti II	1.81	0.27	25	0.11	4.95
Cr	1.83	−0.40	5	0.20	5.64
Fe I	4.09	0.00	98	0.24	7.50
Fe II	4.08	−0.01	11	0.14	7.50
Co	1.64	0.06	1	0.23	4.99
Ni	2.75	−0.06	2	0.16	6.22
Zn	1.62	0.47	2	0.09	4.56
Sr	−0.25	0.29	2	0.19	2.87
Y	−1.20	0.00	3	0.12	2.21
Zr	−0.54	0.29	2	0.17	2.58
Ba	−0.92	0.31	3	0.14	2.18
La	−1.60	0.71	2	0.16	1.10
Ce	−1.47	0.36	2	0.13	1.58
Pr	−1.78	0.91	1	0.15	0.72
Nd	−1.47	0.52	4	0.16	1.42
Sm	−1.67	0.78	2	0.17	0.96
Eu	−1.73	1.16	1	0.14	0.52
Dy	−1.35	0.96	1	0.15	1.10

Carbon. The carbon abundance of LAMOST J110901.22+075441.8 was derived by matching the observed CH $A-X$ band at 4310 Å (i.e., the G-band) to the synthetic spectra. The object shows notable underabundant carbon compared to other $r-$II stars and most of the EMP stars (Fig. 2). The derived abundance ratio [C/Fe]$= -0.57$, which is close to the ratios of the so-called "mixed" EMP giants from the sample of Spite et al. (2005). Such a low carbon abundance ratio is likely to be caused by mixing which has brought processed material from deep layers to the surface. Such cool giants should exhibit enhancement of nitrogen which is probably converted from carbon; however, due to limited wavelength coverage of the snapshot spectrum which does not include the NH or CN lines, we are unable to measure the nitrogen abundance of LAMOST J110901.22+075441.8 with current data.

Sodium. Abundance of Na was derived based on the equivalent width (EW) measurements of the two resonance lines. It can be noticed from Figure 2 that the [Na/Fe] $= 0.58$ of LAMOST J110901.22+075441.8 indicates relative excess compared to other $r-$II stars which normally show solar or a slightly lower [Na/Fe] ratio. The difference may be balanced when the non-LTE (NLTE) correction to sodium abundances are considered, e.g., according to Cayrel et al. (2004), a correction of up to -0.5 dex should be added to the LTE sodium abundance. However, we have only found [Na/Fe] from literatures for a few $r-$II stars, and a larger sample would be needed to make any conclusive remark.

The $\alpha-$elements. For LAMOST J110901.22+075441.8, abundances of four $\alpha-$elements, Mg, Si, Ca and Ti, were derived based on the EW measurements of atomic lines. As shown in Figure 2,

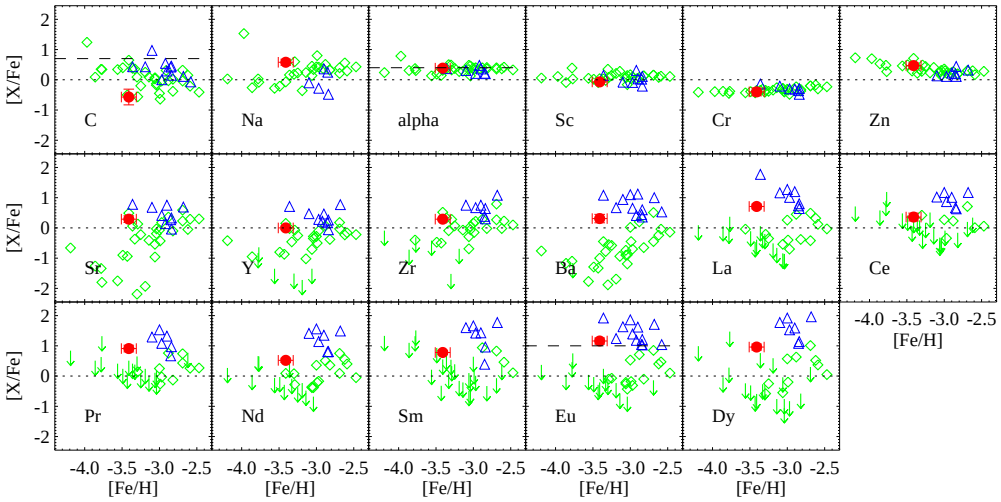

Fig. 2 [X/Fe] vs. [Fe/H] from C through Dy of LAMOST J110901.22+075441.8. Filled circles are abundances of LAMOST J110901.22+075441.8. Triangles are abundance ratios of other $r-$II stars collected from literatures (Hill et al. 2002; Sneden et al. 2003; Honda et al. 2004; Christlieb et al. 2004; Barklem et al. 2005; François et al. 2007; Lai et al. 2008; Sneden et al. 2008; Hayek et al. 2009; Mashonkina et al. 2010; Aoki et al. 2010). Diamonds and downward arrows refer to abundances and upper-limits of metal-poor giants from the "First Stars" project (Cayrel et al. 2004; Spite et al. 2005; François et al. 2007). For C, the dashed line refers to [C/Fe] $\sim +0.7$ which corresponds to the division between the carbon-enhanced and carbon-normal stars (Aoki et al. 2007). For the α-elements, the dashed line refers to the canonical value of [α/Fe] $\sim +0.4$ for halo stars (McWilliam 1997). For Eu, the criterion for $r-$II stars with [Eu/Fe] $\geq +1.0$ (Beers & Christlieb 2005) is also presented with a dashed line for reference.

all the $\alpha-$elements present enhancement relative to iron, with an average [(Mg+Si+Ca+Ti)/Fe] $= +0.37$ which agrees with the canonical value of [α/Fe] $\sim +0.4$ for halo stars (McWilliam 1997).

Scandium and iron−peak elements. Except for V whose atomic lines are not covered and Mn for which only one line with a distorted feature could be found, the abundance of elements in the nuclear charge ranging from $Z = 21$ through 28 were determined for LAMOST J110901.22+075441.8. The abundance ratios of Sc, Co and Ni to iron are about the solar value. Cr is deficient relative to iron and solar ratios, with [Cr/Fe] $= -0.40$, while Zn is overabundant relative to iron with [Zn/Fe] $= +0.47$. These abundance ratios in LAMOST J110901.22+075441.8 agree well with the general trend of EMP halo stars with similar metallicities (with Sc, Cr and Zn shown in Fig. 2 as examples).

In general, we found that the element abundance pattern of LAMOST J110901.22+075441.8 in the C−Zn range resembles the "normal" pattern of halo EMP stars, except that it shows a quite low C abundance and relatively large [Na/Fe]. The underabundance in carbon is presumably due to the fact that it is a more evolved star compared with EMP stars with higher temperatures. The overabundance in sodium may be explained by the discrepancy between LTE and NLTE Na abundances for EMP giants.

3.2 Heavy Elements: Strontium through Dysprosium

We determined abundances of LAMOST J110901.22+075441.8 for 11 heavy elements, including three light trans-iron elements and eight elements in the region of the second r-process peak. The

elements representing the third peak could not be measured, because the wavelength coverage of our spectrum did not include any strong lines for measurements.

The light trans-iron elements. Three elements were measured in the region of the first peak with $38 \leq Z \leq 46$, including Sr, Y and Zr. The abundance of Sr was measured by spectral synthesis of the two strongest resonance lines, Sr II 4077 and 4215 Å. Both of these lines are affected by HFS of the odd isotope ^{87}Sr, and a fraction of 0.22 was adopted for this isotope for synthesis, according to Arlandini et al. (1999) for a pure r-process production of strontium. The correction for HFS and isotopic splitting has resulted in an increase of 0.15 dex for the abundance of Sr, i.e. from -0.25 to -0.10. For Y and Zr, the abundances were derived from the EWs of three and two isolated and clear atomic lines, respectively. Abundances of these elements in LAMOST J110901.22+075441.8 are quite similar to other $r-$II stars, and are higher than the average abundance ratio of "normal" EMP halo stars with similar metallicities (Fig. 2).

The second r-process peak elements. In the region of the second peak, abundances were determined for eight elements, Ba, La, Ce, Pr, Nd, Sm, Eu and Dy. Four isolated barium lines could be measured for LAMOST J110901.22+075441.8, including the Ba II 4554 Å resonance line and the three subordinate lines, Ba II 5853, 6141 and 6497 Å. The three subordinate lines are almost free from HFS effects, and derive quite similar Ba abundances with a difference of about 0.01 dex. However, the resonance line is strongly affected by HFS. Even if we take the HFS splitting for spectral synthesis into account, the Ba II 4554 Å line still results in a Ba abundance that is 0.20 dex higher than that from the subordinate lines. We suspect that this difference is mainly caused by the NLTE effect (Mashonkina & Christlieb 2014), which is not included in our analysis for this paper. Therefore, the adopted Ba abundance of LAMOST J110901.22+075441.8 was solely based on the three subordinate lines. HFS splitting was also accounted for in La (Lawler et al. 2001a), which resulted in a difference of 0.3 dex in $\log \epsilon$(La). Europium is another element for which HFS and isotope splitting has been accounted for. Eu II 4129 Å is the only europium line detected in the spectrum, which consists of more than 30 components in total. The Eu abundance of LAMOST J110901.22+075441.8 was thus derived by synthesizing the Eu II 4129 Å line, taking the HFS data from Lawler et al. (2001b) and the meteoritic isotopic abundance ratio of ^{151}Eu : ^{153}Eu = 47.8 : 52.2. As shown in Figure 2, abundance ratios of the second peak elements relative to iron for LAMOST J110901.22+075441.8 are notably higher than those for normal EMP giants with similar metallicities.

4 HEAVY-ELEMENT ABUNDANCE PATTERN OF LAMOST J110901.22+075441.8

LAMOST J110901.22+075441.8 is the cool $r-$II giant with the lowest metallicity yet known. Figure 3 compares its abundance pattern of heavy elements with those of two well-studied cool $r-$II giants with $T_{\rm eff}$<5000 K, CS 22892−052 (Sneden et al. 2003) and CS 31082−001 (Hill et al. 2002). Abundances of the comparison stars are scaled to match the abundance of La in LAMOST J110901.22+075441.8. Previous studies have indicated that the pattern of heavy-element abundances in these two comparison stars is tracing the main component of the r-process (Sneden et al. 2003; Roederer et al. 2014). It is clear from the comparison that in the range from Sr to Dy, the abundance pattern of the neutron-capture elements in LAMOST J110901.22+075441.8 is very similar to the two cool $r-$II giants, and thus the main r-process. For example, the dispersion in the average difference of $\log \epsilon$(x) values between LAMOST J110901.22+075441.8 and the two comparison $r-$II stars is about 0.19 dex (vs. CS 22892−052) and 0.15 dex (vs. CS 31082−001), respectively, which is comparable to the 1σ error in our elemental abundance determinations. The similar chemical abundance pattern observed in neutron-capture elements suggests that there should be a common origin for these elements in the classical r-process.

For comparison, the SSr patterns predicted by Bisterzo et al. (2014) and Arlandini et al. (1999) are also displayed in Figure 3, respectively as solid and dashed lines. These two sets of solar $r-$components are very similar except for elements with a significant contribution of s-process to

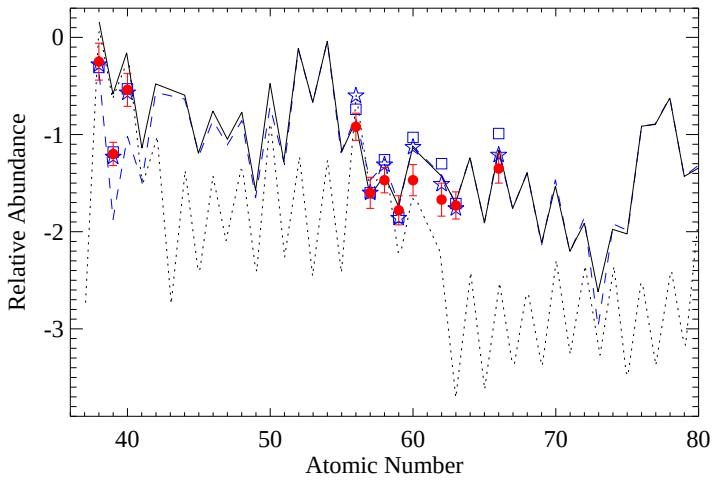

Fig. 3 Heavy-element abundance patterns of LAMOST J110901.22+075441.8 (*filled circles*) and r-II stars with $T_{\rm eff}$ cooler than 5000 K, including CS 22892−052 (Sneden et al. 2003, *squares)* and CS 31082−001 (Hill et al. 2002, *stars)*. The element abundances are scaled to match La in LAMOST J110901.22+075441.8. The solid curve refers to the SSr abundance patterns from Bisterzo et al. (2014), and the dashed and dotted lines indicate those of the $r-$ and s-process components in the SSr from Arlandini et al. (1999), respectively.

their solar abundances, especially for the light trans-iron elements such as Sr, Y and Zr. However, as discussed in Mashonkina & Christlieb (2014), it would be difficult to make a firm conclusion about the relation between $r-$II stars and the solar r-process shown by light trans-iron elements, due to the large uncertainty in the solar $r-$residuals. When compared to the predicted abundances by Bisterzo et al. (2014) and those by Arlandini et al. (1999), the elements in the range from Ba through Dy in LAMOST J110901.22+075441.8 are found to match the scaled SSr pattern very well, with a dispersion of 0.13 dex and 0.16 dex respectively, about the average abundance differences for the eight second peak elements. The observed match is in line with previous studies on other r-process rich stars, and provides additional evidence for the universal production ratio of these elements during the evolution of the Galaxy.

Previous studies on metal-poor halo stars suggest that there exist distinct mechanisms involved in the production of light trans-iron elements as well as heavier elements beyond Ba (Aoki et al. 2005; François et al. 2007; Mashonkina et al. 2007). By choosing Sr (Zr) and Eu to represent the first and second neutron-capture element peaks, we could inspect the Sr/Eu and Zr/Eu abundance ratios of the $r-$II stars. Figure 4(a) and (b) show the distribution of abundance ratios of log Sr/Eu and log Zr/Eu for known $r-$II stars including LAMOST J110901.22+075441.8. The average values of log Sr/Eu and log Zr/Eu are 1.39±0.11 and 1.32±0.12 (dotted lines) respectively, which are consistent with the results of previous studies (e.g. Mashonkina et al. 2010), and are relatively smaller than those of normal EMP stars. Also, an average value for log Ba/Eu of 0.98±0.11 (the dotted line in Fig. 4(c)) is derived from the 12 $r-$II stars, which agrees well with the predicted value of 0.93 for the pure r-process production of heavy elements (Arlandini et al. 1999), indicating that the environment from which these stars were formed only contained a small amount of $s-$nuclei. The distribution of the abundance ratios as shown in Figure 4 also suggests there is a common origin for the first and second r-process peak elements in strongly r-process enhanced stars.

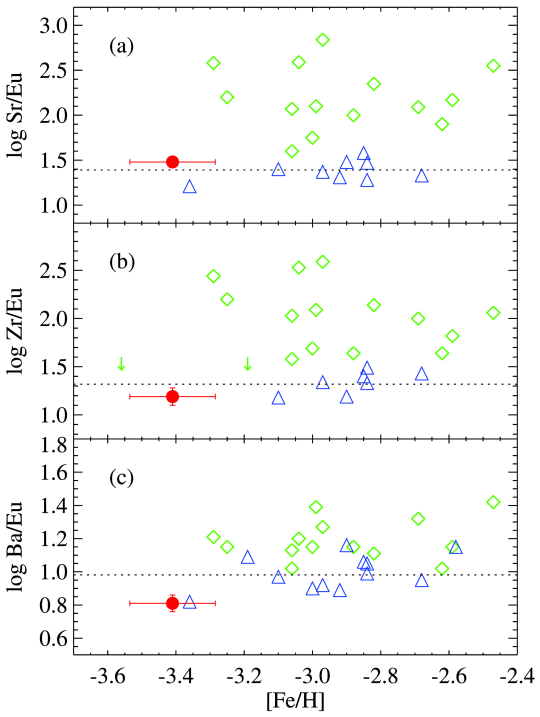

Fig. 4 The distribution of the log Sr/Eu (a), log Zr/Eu (b) and log Ba/Eu (c) abundance ratios in $r-$II stars (LAMOST J110901.22+075441.8 shown as filled circles, and $r-$II stars from the literature shown as triangles), and regular EMP giants from "First Stars" (François et al. 2007, diamonds represent abundances and arrows denote upper limits). The dotted lines indicate the average abundance ratio of the known $r-$II stars, as described in the text.

5 CONCLUSIONS

LAMOST J110901.22+075441.8 has been selected as a candidate of an EMP star from the LAMOST spectroscopic survey, and was followed-up by obtaining its high-resolution spectrum with Subaru/HDS. The relatively high quality Subaru/HDS spectrum enabled us to determine accurate parameters and elemental abundances for 23 species, including 11 elements in the nuclear charge range of $Z = 38 - 66$ which covers the light trans-iron and second r-process peak elements. Detailed abundance analysis confirms that LAMOST J110901.22+075441.8 is a strongly r-process enhanced EMP star having [Eu/Fe] $= +1.16$. It is also found that in the range from Sr to Dy, LAMOST J110901.22+075441.8 presents very similar abundance patterns of the elements to the well studied cool $r-$II giants, CS 22892−052 and CS 31082−001, whose patterns of heavy elements can be explained well by a main component of the r-process. Therefore LAMOST J110901.22+075441.8 is a newly discovered member of the small sample of currently known $r-$II stars, with the lowest metallicity of [Fe/H] ~ -3.4 among $r-$II giants.

The abundance pattern from Ba to Dy in LAMOST J110901.22+075441.8 can be matched well by the scaled solar r-process pattern prediction by Arlandini et al. (1999) and Bisterzo et al. (2014). However, the large uncertainty in the solar $r-$residuals for the first r-process peak elements leads to difficulties in drawing any conclusion concerning the relation between the light trans-iron elements in LAMOST J110901.22+075441.8 (and other $r-$II stars) and the solar r-process.

Apart from different metallicities, LAMOST J110901.22+075441.8 presents quite similar abundance ratios of Sr/Eu and Zr/Eu compared with previously well studied $r-$II stars, and further confirms that LAMOST J110901.22+075441.8 is a member of the group of $r-$II stars. LAMOST J110901.22+075441.8 turns out to be the lowest metallicity $r-$II star with measured Zr abundance. The extreme enhancement in [Eu/Fe] and low Sr/Eu (Zr/Eu, Ba/Eu as well) in LAMOST J110901.22+075441.8 indicates a single or very few nucleosynthesis events as is the case for other $r-$II stars.

However, due to limited wavelength coverage of the snapshot spectrum, our analysis does not include any elements heavier than Dy. To investigate abundance of the third r-process peak elements of LAMOST J110901.22+075441.8, we will need to further obtain spectra with higher quality and higher resolution which cover the UV band to investigate the chemical abundances of heavier elements beyond Dy.

Acknowledgements We are grateful to the anonymous referee for helping to improve the paper. H. N. L. and G. Z. acknowledge supports by the National Natural Science Foundation of China (Grant Nos. 11103030, 11233004 and 11390371). W. A. and T. S. are supported by the JSPS Grant-in-Aid for Scientific Research (S: 23224004). S. H. is supported by the JSPS Grant-in-Aid for Scientific Research (c:26400231). N. C. acknowledges support from Sonderforschungsbereich 881 "The Milky Way System" (subproject A4) of the German Research Foundation (DFG). The Guo Shou Jing Telescope (the Large Sky Area Multi-Object Fiber Spectroscopic Telescope, LAMOST) is a National Major Scientific Project built by the Chinese Academy of Sciences. Funding for the project has been provided by the National Development and Reform Commission. LAMOST is operated and managed by National Astronomical Observatories, Chinese Academy of Sciences. This work is based on data collected at the Subaru Telescope, which is operated by the National Astronomical Observatory of Japan.

References

Alonso, A., Arribas, S., & Martínez-Roger, C. 1999, A&AS, 140, 261
Alonso, A., Arribas, S., & Martínez-Roger, C. 2001, A&A, 376, 1039
Aoki, W., Honda, S., Beers, T. C., et al. 2005, ApJ, 632, 611
Aoki, W., Beers, T. C., Christlieb, N., et al. 2007, ApJ, 655, 492
Aoki, W., Beers, T. C., Honda, S., & Carollo, D. 2010, ApJ, 723, L201
Aoki, W., Beers, T. C., Lee, Y. S., et al. 2013, AJ, 145, 13
Arlandini, C., Käppeler, F., Wisshak, K., et al. 1999, ApJ, 525, 886
Asplund, M., Grevesse, N., Sauval, A. J., & Scott, P. 2009, ARA&A, 47, 481
Barklem, P. S., Christlieb, N., Beers, T. C., et al. 2005, A&A, 439, 129
Beers, T. C., & Christlieb, N. 2005, ARA&A, 43, 531
Bisterzo, S., Travaglio, C., Gallino, R., Wiescher, M., & Käppeler, F. 2014, ApJ, 787, 10
Burris, D. L., Pilachowski, C. A., Armandroff, T. E., et al. 2000, ApJ, 544, 302
Castelli, F., & Kurucz, R. L. 2003, in IAU Symposium, 210, Modelling of Stellar Atmospheres, eds. N. Piskunov, W. W. Weiss, & D. F. Gray, 20P
Cayrel, R. 1988, in IAU Symposium, 132, The Impact of Very High S/N Spectroscopy on Stellar Physics, eds. G. Cayrel de Strobel, & M. Spite, 345
Cayrel, R., Depagne, E., Spite, M., et al. 2004, A&A, 416, 1117
Christlieb, N., Beers, T. C., Barklem, P. S., et al. 2004, A&A, 428, 1027
Cui, X.-Q., Zhao, Y.-H., Chu, Y.-Q., et al. 2012, RAA (Research in Astronomy and Astrophysics), 12, 1197
François, P., Depagne, E., Hill, V., et al. 2007, A&A, 476, 935
Frebel, A., Casey, A. R., Jacobson, H. R., & Yu, Q. 2013, ApJ, 769, 57
Frebel, A., Christlieb, N., Norris, J. E., et al. 2007, ApJ, 660, L117

Goriely, S., Sida, J.-L., Lemaître, J.-F., et al. 2013, Physical Review Letters, 111, 242502
Hayek, W., Wiesendahl, U., Christlieb, N., et al. 2009, A&A, 504, 511
Hill, V., Plez, B., Cayrel, R., et al. 2002, A&A, 387, 560
Honda, S., Aoki, W., Kajino, T., et al. 2004, ApJ, 607, 474
Lai, D. K., Bolte, M., Johnson, J. A., et al. 2008, ApJ, 681, 1524
Lawler, J. E., Bonvallet, G., & Sneden, C. 2001a, ApJ, 556, 452
Lawler, J. E., Wickliffe, M. E., den Hartog, E. A., & Sneden, C. 2001b, ApJ, 563, 1075
Li, H.-N., Zhao, G., Christlieb, N., et al. 2015, ApJ, 798, 110
Liu, X. W., Zhao, G., & Hou, J. L. 2015, RAA (Research in Astronomy and Astrophysics), 15, 1089
Luo, A.-L., Zhang, H.-T., Zhao, Y.-H., et al. 2012, RAA (Research in Astronomy and Astrophysics), 12, 1243
Luo, A.-L., Zhao, Y.-H., Zhao, G., et al. 2015, RAA (Research in Astronomy and Astrophysics), 15, 1095
Mashonkina, L., & Christlieb, N. 2014, A&A, 565, A123
Mashonkina, L., Christlieb, N., Barklem, P. S., et al. 2010, A&A, 516, A46
Mashonkina, L. I., Vinogradova, A. B., Ptitsyn, D. A., Khokhlova, V. S., & Chernetsova, T. A. 2007, Astronomy Reports, 51, 903
McWilliam, A. 1997, ARA&A, 35, 503
Roederer, I. U., Cowan, J. J., Preston, G. W., et al. 2014, MNRAS, 445, 2970
Sneden, C. 1973, ApJ, 184, 839
Sneden, C., Preston, G. W., McWilliam, A., & Searle, L. 1994, ApJ, 431, L27
Sneden, C., McWilliam, A., Preston, G. W., et al. 1996, ApJ, 467, 819
Sneden, C., Cowan, J. J., Lawler, J. E., et al. 2003, ApJ, 591, 936
Sneden, C., Cowan, J. J., & Gallino, R. 2008, ARA&A, 46, 241
Sobeck, J. S., Kraft, R. P., Sneden, C., et al. 2011, AJ, 141, 175
Spite, M., & Spite, F. 1978, A&A, 67, 23
Spite, M., Cayrel, R., Plez, B., et al. 2005, A&A, 430, 655
Woosley, S. E., Wilson, J. R., Mathews, G. J., Hoffman, R. D., & Meyer, B. S. 1994, ApJ, 433, 229
Zhao, G., Chen, Y.-Q., Shi, J.-R., et al. 2006, ChJAA (Chin. J. Astron. Astrophys.), 6, 265
Zhao, G., Zhao, Y.-H., Chu, Y.-Q., Jing, Y.-P., & Deng, L.-C. 2012, RAA (Research in Astronomy and Astrophysics), 12, 723